

Demonstrating Dilute-Tin Alloy SiGeSn for Use in Multijunction Photovoltaics: Single- and Multijunction Solar Cells With a 1.0-eV SiGeSn Junction

Radek Roucka, Andrew Clark, Tom Wilson, Tomos Thomas, Markus Führer, Nicholas Ekins-Daukes, Andrew Johnson, Rick Hoffman, Jr., and David Begarney

Abstract—SiGeSn ternary alloys offer a means to fabricate a 1.0-eV subcell junction for inclusion in a multijunction solar cell. The main advantage of the SiGeSn alloy is a tuneable bandgap energy and variable lattice parameter, enabling the material to be integrated into the existing lattice-matched multijunction architectures. Recent growth, structural, optical, and device results from SiGeSn material, with energy gaps in the vicinity of 1.0 eV and lattice matched to Ge substrates, are presented. An all lattice-matched InGaP/InGaAs/SiGeSn triple-junction cell is presented and compared with a conventional InGaP/InGaAs/Ge solar cell. Comparable short-circuit current values of 13.9 mA/cm² are obtained for both devices under the AM1.5G spectrum, whereas the open-circuit voltage and fill factor are reduced in the device with the SiGeSn subcell. Peak external quantum efficiency in the SiGeSn single junction in excess of 80% is realized, placing a lower limit on the base minority hole diffusion length of 5 μm with surface recombination velocities in close agreement to those found in bulk Ge material.

Index Terms—Concentrator photovoltaics, highly mismatched alloys, multijunction solar cell, silicon–germanium–tin, single-junction solar cell, III–V semiconductors.

I. INTRODUCTION

III–V multijunction solar cells offer exceptionally high power conversion efficiency and, hence, find application in areas where efficiency is of paramount importance, for example terrestrial concentrator photovoltaics or space. The potential efficiency scales with the number of active subcells with up to six junctions demonstrated to date [1]. At present, commercially available triple-junction (3J) solar cells can deliver 40% power conversion efficiency [2] under concentrated sunlight,

rising to 46.1% for the best quad-junction device fabricated in a research laboratory [3]. At present, the principal weakness in these multijunction solar cells is fabricating lattice-matched semiconductor alloys with bandgap energies around 1 eV. Conventionally, dilute nitride materials have been employed for this purpose, i.e., InGaNAsSb [4] and InGaNAs [5], achieving 43% under concentration [6] when grown by molecular beam epitaxy. However, high p-type background doping, on the order of 10¹⁷ cm⁻² [7], has been observed in metal–organic vapor phase epitaxy (MOPVE) grown material, presenting difficulties in achieving optimum carrier concentrations and minority carrier mobility [8]. At present, MOVPE-grown 1-eV subcells involve using metamorphic InGaAs layers grown in an inverted structure [9]. These structures are grown on thick graded buffer layers, and the inverted sequence ensures that residual threading dislocations do not propagate into the higher bandgap subcells, although it does require the substrate to be removed.

A viable alternative to all these compounds are group IV ternary alloys of Si, Ge, and Sn, which allow for both tuneable bandgap and variable lattice parameter at the same time [10]. These alloys have a diamond crystal structure with no site preference for any of the constituent elements. Therefore, by fixing the lattice parameter to a desired value, one can vary the alloy composition over a broad range, which simultaneously determines the bandgap value. Although, in this study, we present results for indirect gap SiGeSn, parameterization of the SiGeSn bandgap indicates that the material moves from indirect to direct gap for Sn fractions in excess of 13%, while still remaining lattice matched to Ge [11]. As a result, SiGeSn has seen renewed interest in recent years as a potential direct-gap alloy for Si-based photonic applications [12]. Here, we consider the application of this alloy as a potential semiconductor material in a multijunction solar cell based on Ge or GaAs substrates commonly used for fabricating multijunction solar cells. When constrained to the Ge or GaAs lattice constant, SiGeSn alloys can provide bandgap energies between 0.8 and 1.2 eV [12]. An initial study demonstrating the feasibility of a SiGeSn 1.0-eV junction lattice-matched to Ge has shown promising device results with a peak single-junction (1J) external quantum efficiency (EQE) in excess of 60% [13].

The principal objective of this study is to demonstrate the integration of SiGeSn alloys in an existing InGaP/GaAs-based

Manuscript received December 10, 2015; revised February 5, 2016 and April 7, 2016; accepted April 12, 2016. Date of publication May 25, 2016; date of current version June 17, 2016.

R. Roucka and A. Clark are with Translucent Inc., Palo Alto, CA 94303 USA (e-mail: radek@translucentinc.com; andrew@translucentinc.com).

T. Wilson, T. Thomas, M. Führer, and N. Ekins-Daukes are with the Blackett Laboratory, Department of Physics, Imperial College London, London SW7 2AZ, U.K. (e-mail: t.wilson14@imperial.ac.uk; tdt08@ic.ac.uk; markus.fuhrer01@imperial.ac.uk; n.ekins-daukes@imperial.ac.uk).

A. Johnson, R. Hoffman, Jr., and D. Begarney are with IQE PLC, Cardiff CF3 0LW, U.K. (e-mail: AJohnson@IQEP.com; rhoffman@iqep.com; dbegarney@iqep.com).

Color versions of one or more of the figures in this paper are available online at <http://ieeexplore.ieee.org>.

Digital Object Identifier 10.1109/JPHOTOV.2016.2559785

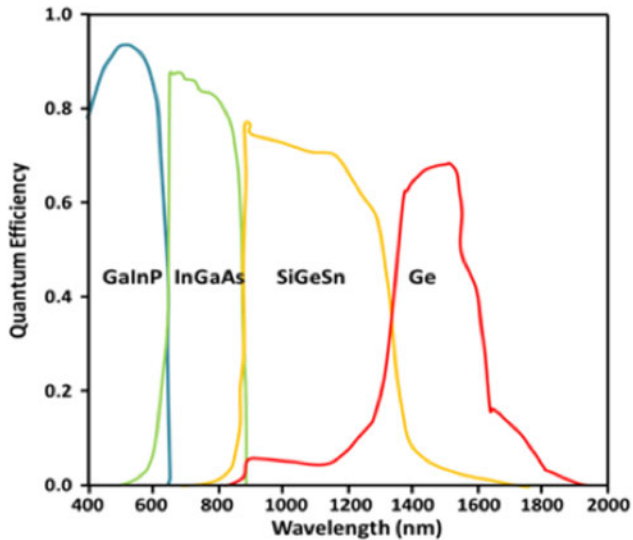


Fig. 1. Calculated EQE for lattice-matched $\text{Ga}_{0.51}\text{In}_{0.49}\text{P}/\text{In}_{0.01}\text{Ga}_{0.99}\text{As}/\text{Ge}_{0.879}\text{Si}_{0.095}\text{Sn}_{0.026}/\text{Ge}$ four-junction cell that is predicted to increase 1-sun efficiency by 5% absolute over $\text{Ga}_{0.51}\text{In}_{0.49}\text{P}/\text{In}_{0.01}\text{Ga}_{0.99}\text{As}/\text{Ge}$.

multijunction solar cell architecture. Starting from a simulation of the potential that a SiGeSn component junction can hold, we then experimentally demonstrate the performance of both a SiGeSn 1J component and a lattice-matched 3J device with SiGeSn bottom cell. In our study, we employed a simple 3J design based on the InGaP/InGaAs/Ge lattice-matched cell. By interpolating published SiGeSn absorption coefficient data [12], we calculated the enhancement possible by including a fourth subcell made from SiGeSn alloy and optimized the overall cell performance with respect to the SiGeSn compositions and thicknesses. For simplicity, the multijunction solar cell was calculated under AM1.5D spectral profile, 1-sun irradiance, and a 65-nm-thick Si_3N_4 antireflective coating was included. The simulated EQE plot for each junction is shown in Fig. 1. This was calculated using an analytical solution to the semiconductor drift-diffusion equations for a p-n diode [14]. The current-matched current density of $12.7 \text{ mA}/\text{cm}^2$ was obtained for 2.5- μm -thick $\text{Ge}_{0.832}\text{Si}_{0.132}\text{Sn}_{0.036}$ alloy with absorption threshold of 0.95 eV (1300 nm). Introduction of such junction into the lattice-matched stack can increase the 1-sun performance of the cell from 34% up to 39% at ideal conditions. With additional concentration of 100 suns, the efficiencies can reach 50%.

II. SiGeSN GROWTH

SiGeSn alloys were synthesized using ultra-high vacuum chemical vapor deposition (UHV-CVD) process utilizing Ge_2H_6 , Si_3H_8 and SnD_4 precursors. Hydrogen was used as the carrier gas. The reactor used was a custom-made horizontal hot wall UHV-CVD system [15]. Commercially available SnD_4 precursor requires low-temperature storage, and a point-of-use delivery system was developed for its use in the growth reactor. Typical SiGeSn layer growth temperatures were

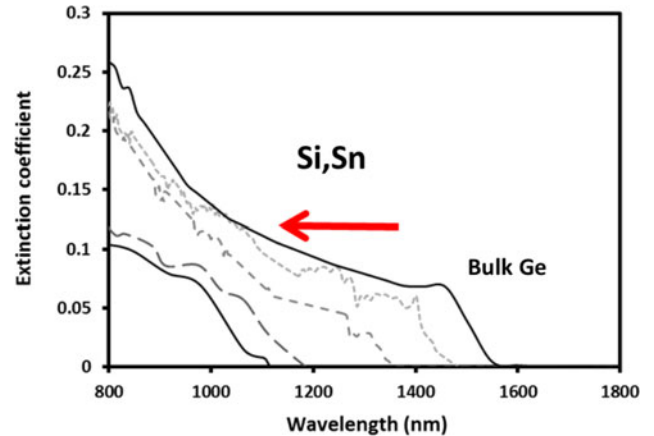


Fig. 2. Extinction coefficient obtained from ellipsometric data for a series of SiGeSn alloys with increasing Si and Sn content grown on Ge substrates, with a sample of bulk Ge for reference, covering the desired 0.67–1.1 eV energy range. The content of Si and Sn was controlled by flows of the CVD precursors so that the lattice parameter of the resulting alloy was matched to that of Ge substrate. The red arrow indicates the direction of increased Si and Sn flow.

in the range of 300–450 °C, and the growth pressures reached 200–600 mtorr. We have grown all group IV alloy films on 100-mm-diameter Ge(1 0 0) substrates, which were miscut by 6° toward the $\langle 1 \ 1 \ 1 \rangle$ direction. This type of template is required by the subsequent MOVPE growth of III–V compounds in order to eliminate the formation of antiphase boundaries. An additional layer of p-type ($n = 5\text{--}8 \times 10^{18} \text{ cm}^{-3}$) SiGeSn with a bandgap of approximately 1.05 eV, wider than the targeted 1.0 eV of the active layer, was grown to act as a back-surface field to limit the diffusion of minority carriers into the Ge substrate. The typical growth rates of SiGeSn varied from 0.3 to 1 $\mu\text{m}/\text{h}$ depending upon the layer composition.

Spectroscopic ellipsometry was used to determine the SiGeSn alloy absorption edge and data taken for a variety of alloy compositions, including a sample of bulk Ge for reference, is shown in Fig. 2. The alloy composition was changed by varying the flow of Si and Sn, and the films were determined to be lattice-matched to Ge using X-ray diffraction. Absorption edges spanning the desired bandgap range of 0.67–1.1 eV (1100–1500 nm) were obtained for increasing Si and Sn fractions. The red arrow in Fig. 2 indicates the direction of increasing Si and Sn content in the alloy.

X-ray diffraction scans around the (0 0 4) Ge/SiGeSn reflection revealed that the crystalline quality of the SiGeSn layers is very high. The full-width at half-maximum of the double-crystal rocking curve measured from the alloy peak (54 arcsec) was comparable with that of the substrate Ge (35 arcsec) indicating very low density of defects. The layer quality was further assessed using transmission electron microscopy, as shown in Fig. 3, where the interface between the Ge substrate and the 2.5- μm -thick SiGeSn overlayer is barely discernable.

Smooth surfaces were achieved after the SiGeSn epitaxy and atomic force microscopy measurements of surface roughness yielded RMS values of only 0.26 nm on $20 \times 20 \mu\text{m}$ scan area. The miscut of the surface with respect to the $\langle 0 \ 0 \ 1 \rangle$ direction

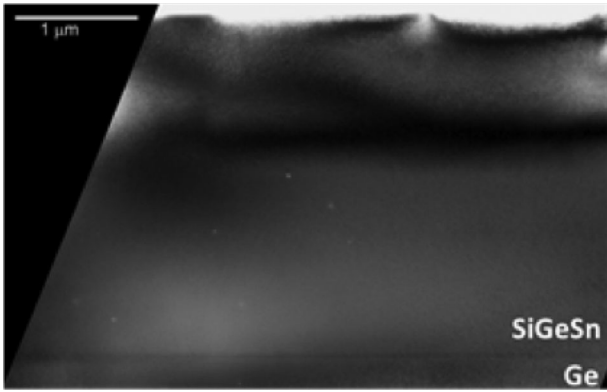


Fig. 3. Cross-sectional TEM image shown is a bright field mode in the $\langle 110 \rangle$ projection of 2.5- μm -thick SiGeSn alloy layer grown on Ge substrate shows no threading defects.

was preserved as well within 0.5° making the SiGeSn suitable for subsequent MOVPE growth.

III. SOLAR CELL GROWTH AND FABRICATION

Since we have not yet developed a tunnel junction between the Ge substrate and SiGeSn layer, we have omitted the bottom Ge subcell formation and concentrated only on 1J SiGeSn cells and 3J InGaP/InGaAs/SiGeSn cell stacks. The SiGeSn was doped p-type to a level consistent with that used in a typical Ge subcell. The carrier concentration was measured to be $1 \times 10^{18} \text{ cm}^{-3}$, as determined by secondary ion mass spectrometry (not shown here). The resulting SiGeSn/Ge wafers were inserted into a Veeco E450 MOVPE tool for growth of 1J and 3J solar cell structures, with pure Ge substrates of the same specification as those used for the SiGeSn layers being inserted into the MOVPE reactor in the same growth run as control samples. This way, the SiGeSn/Ge samples were used as virtual Ge substrates, and a standard III-V on Ge nucleation process, used to diffuse the n-type emitter layer into the p-type Ge substrate, was used for both types of sample. The Ge and SiGeSn subcell emitters were fabricated through controlled diffusion of Group V atomic species during the III-V nucleation process by MOVPE. This process has been developed for the manufacture of conventional InGaP/GaAs/Ge solar cells and typically has an emitter depth of $\approx 0.5 \mu\text{m}$ in pure p-type Germanium. An identical process was used for both Ge and SiGeSn subcells in this study, although it is expected that the different diffusion behavior of Group V species in Silicon containing material may well have an effect on the overall performance of the SiGeSn subcell. These diffusion effects are under investigation and will be reported elsewhere when completed. The 1J samples were grown using only an AlInP/InGaAs window/contact structure on top of the III-V nucleation layer, but the 3J structure utilized a conventional Ge/InGaAs/InGaP architecture, using a layer design that had previously given good solar cell performance when fabricated into devices on Ge substrates. The resulting SiGeSn and Ge 1J and 3J epitaxial structures were fabricated into approximately 1- cm^2 solar cell devices under subcontract using a

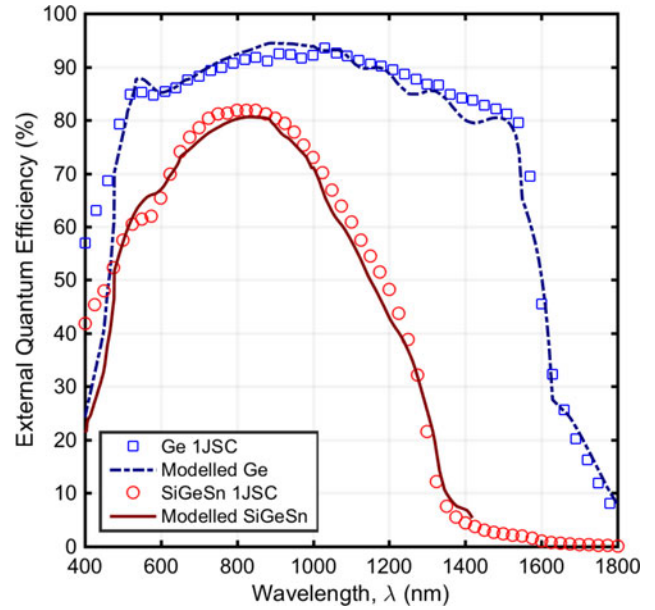


Fig. 4. EQE of 1J Germanium and SiGeSn devices with experimental data displayed as markers modeled fits to the EQE as solid lines. The parameters for the EQE fits are given in Table I.

commercial process and manufactured with a single-layer Si_3N_4 antireflection coating.

IV. EXPERIMENTAL DEVICE RESULTS

A. Single-Junction Solar Cells

EQE measurements were carried out using a quartz-halogen light source, dispersed through a 0.3-m spectrometer. The generated photocurrent was recorded using a standard lock-in technique and the EQE calculated from the known photocurrent responsivity of reference Si and Ge photodiodes. Fig. 4 illustrates EQE measurements of both the SiGeSn 1J and a reference 1J Germanium device. The SiGeSn alloy exhibits a good EQE response, with a peak of approximately 80% observed at 800 nm. This value is comparable with the Germanium reference device, although we observe a significant reduction in EQE above 800 nm toward the band edge. This is partly due to the single layer antireflection coating, to which 0.48 mA/cm^2 (under AM1.5G) is lost due to reflection.

The EQE of the cells has been modeled using analytical solutions to the semiconductor transport equations for a p-n junction [16], enabling useful information such as minority carrier transport properties to be extracted. It is assumed that there is a space-charge region over which each absorbed photon contributes one electron to I_{SC} . Either side of this are quasi-neutral regions within which minority carriers diffuse to the junction with a characteristic diffusion length. As the junction in the SiGeSn cells was formed in a similar way to those of a standard Ge bottom subcell, first, the germanium EQE was modeled, the results of which are shown in Fig. 4. The best fit was obtained with base minority carrier diffusion length of $100 \mu\text{m}$, emitter minority carrier diffusion length of order $1 \mu\text{m}$, and surface

TABLE I
PARAMETERS USED TO FIT THE EQE OF GE AND SiGeSn 1J CELLS AS WELL AS 3J SiGeSn SUBCELL

Device	Front surface recombination velocity (cm/s)	Electron (base) diffusion length (μm)	Hole (emitter) diffusion length (μm)
Germanium	5×10^4	100	< 1
SiGeSn	5×10^4	> 5	0.35

TABLE II
IMPORTANT SOLAR CELL PARAMETERS EXTRACTED FROM 1J I - V MEASUREMENT UNDER AM1.5G ILLUMINATION

Device	J_{sc} (mA/cm ²)	V_{oc} (V)	Fill Factor $FF(\%)$
Germanium	57.67	0.247	67.47
SiGeSn	30.12	0.230	65.37

recombination of 5×10^4 cm/s. Modeling the SiGeSn junction proceeded by assuming similar surface recombination and doping to the Ge junction. Furthermore, the space-charge properties were determined using effective masses and bandgaps reported by Soref and Perry [10].

An absorption coefficient was determined from the ellipsometry measurements shown in Fig. 2, and the reflectance of the devices was measured at normal incidence. At higher incident photon energies than those shown in Fig. 2, Germanium-like absorption was assumed for the SiGeSn alloy, an assumption consistent with observations of the dielectric function of the alloy. The modeled SiGeSn EQE is shown in Fig. 4. A value of 350-nm minority hole diffusion length in the emitter was found from the fits of the experimental data. Due to the fact that the SiGeSn cells are optically thin, only a lower bound may be placed on the base minority carrier diffusion length. This was found to be on the order of $5 \mu\text{m}$. This value suggests that carrier transport is sufficiently good and increasing the thickness of the SiGeSn base may further improve the short-circuit current of this subcell. Full EQE parameters are found in Table I.

To complement the EQE measurements, we show the light I - V characteristic response, measured under single-sun illumination conditions, for both the SiGeSn and Germanium reference devices in Fig. 5. A dual-source TS-Space Systems Class-A solar simulator, using both metal halide and quartz halogen lamps, was used to provide a close match to the terrestrial AM1.5G spectrum in the wavelength range 320–2200 nm [17]. The short-circuit current for the SiGeSn device is just over half that exhibited by the reference Germanium cell. A reduced short-circuit current is to be expected given the measured EQE response in Fig. 4. It is important to note that the observed open-circuit voltage (V_{OC}) for SiGeSn does not exceed that of Germanium. Using the reciprocity relation between photovoltaic EQE and electroluminescence, reported by Rau [18], we estimate the V_{OC} in the radiative limit from the SiGeSn EQE shown in Fig. 4 to be approximately 0.66 V, which is 0.29 V lower than the estimated bandgap energy of 0.95 eV. The reduction in voltage can be attributed to the presence of absorp-

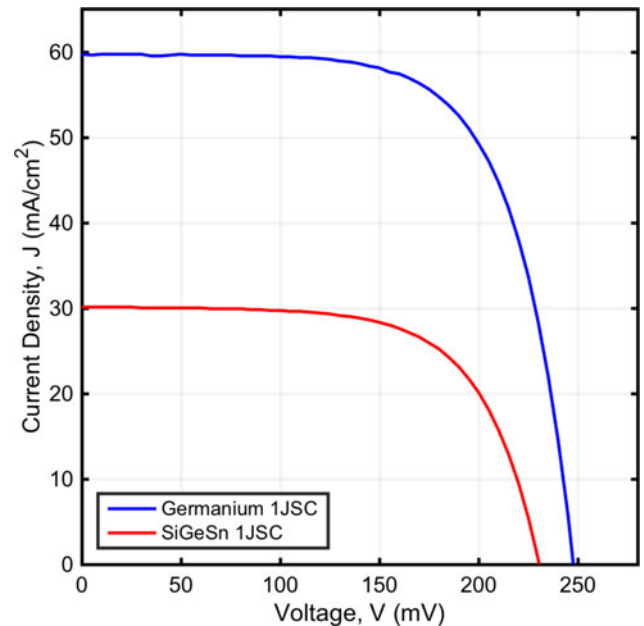


Fig. 5. 1J light I - V characteristics under AM1.5G single-sun illumination for SiGeSn and the Germanium reference device. Performance parameters can be found in Table II.

tion in subbandgap tail states in the material, evidence of which can be seen in the EQE above 1300 nm. The effect of these tail states on the SiGeSn voltage can be addressed with future growth optimization, which will also help reduce unwanted excessive bulk and surface recombination that will also contribute to the low V_{OC} . Given the relatively novel state of the alloy, the initial results shown here highlight that, with further growth optimization, there is the potential for 1.0-eV SiGeSn with a direct bandgap to generate a V_{OC} in the vicinity of 0.6 V, assuming a bandgap voltage offset in the region of 0.4 V [19].

B. Triple-Junction Solar Cells

The EQE for two 3J solar cells, one conventional InGaP/InGaAs/Ge cell and an InGaP/InGaAs/SiGeSn cell grown on Ge, is shown in Fig. 6. The SiGeSn EQE has been modeled using the same parameters as the 1J (discussed above and given in Table I) and is additionally shown. The peak EQE for the Germanium-based control cell is approximately 80%, while the peak EQE in the SiGeSn-based device is in excess of 70% for all junctions. These results indicate that the SiGeSn junction has been successfully integrated into the conventional InGaP/InGaAs multijunction architecture without degradation of the InGaP/InGaAs subcells, and the SiGeSn junction retains the properties of the 1J in this 3J format. The EQE response in the SiGeSn shows a steady decrease from 70% at ≈ 950 nm to roughly 35% at 1350 nm, which differs from the relatively flat response exhibited by the Ge control junction. The $5\text{-}\mu\text{m}$ base diffusion length obtained by fitting the EQE indicates that using a thicker SiGeSn absorbing layer would increase photocurrent generation and improve the infrared wavelength response. The leading edge for absorption appears to cut in at around 1300 nm,

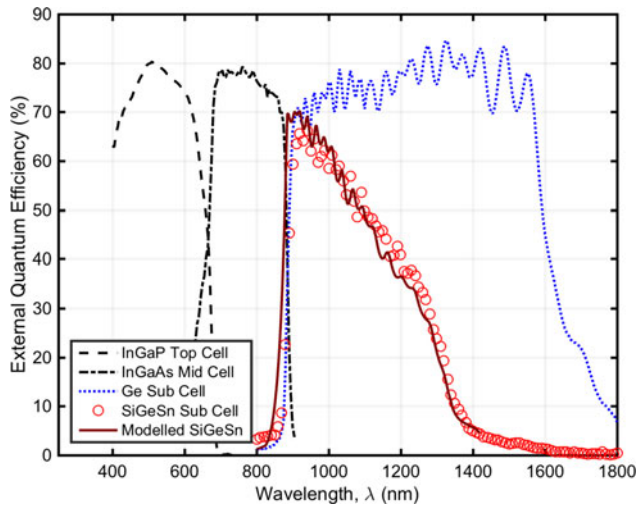


Fig. 6. Experimental EQE for the 3J devices. The plotted InGaP and InGaAs top and middle cells are similar for both devices. A modelled fit to the SiGeSn data is also included; the parameters are given in Table I.

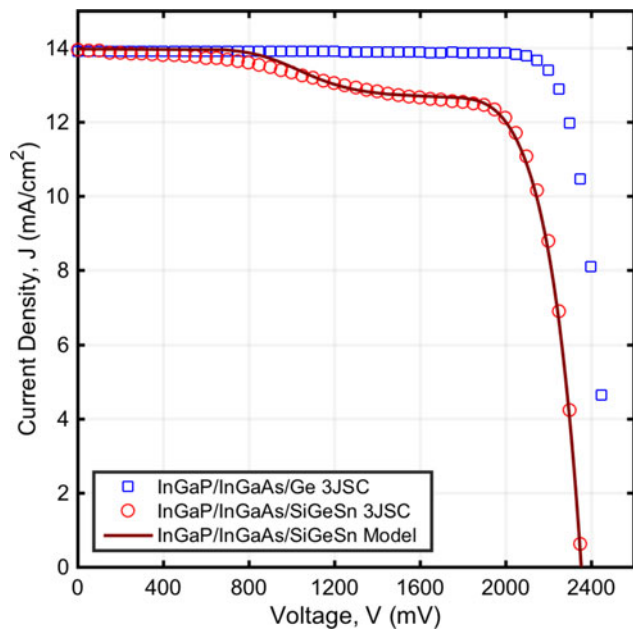


Fig. 7. Experimental light I - V under single-sun illumination conditions for standard Ge- and SiGeSn-based 3J devices. Performance parameters can be found in Table III. Solid line indicates the fit to 3J light I - V including reverse breakdown of the SiGeSn subcell.

which suggests a bandgap energy of 0.95 eV; however, a smaller absorption onset at around 1580 nm may suggest contributions from the indirect bandgap, with energy 0.78 eV.

Fig. 7 depicts light I - V measurements under single-sun AM1.5G illumination conditions for both the 3J Ge control and SiGeSn devices. We observe comparable short-circuit current for both devices and an open-circuit voltage for the SiGeSn cell slightly below that of the Ge control, as expected given the voltage performance of the 1J device shown in Fig. 5. The fill factor for the control cell (84.8%) is typical for a 3J device,

TABLE III
IMPORTANT SOLAR CELL CHARACTERISTICS EXTRACTED FROM 3J LIGHT I - V MEASUREMENTS

Device	J_{sc} (mA/cm ²)	V_{oc} (V)	Fill Factor FF (%)
InGaP/InGaAs/Ge	13.912	2.50	84.8
InGaP/InGaAs/SiGeSn	13.943	2.36	73.7

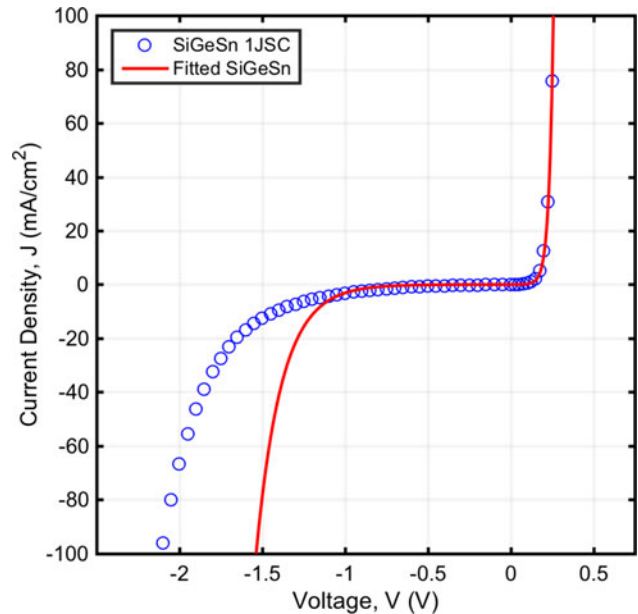


Fig. 8. Measured data (blue open circles) and fitted (solid red line) dark I - V for SiGeSn 1J showing reverse bias breakdown determined from 3J fitting. Fitted breakdown differs from the breakdown observed in the 1J measurement. Intercell variation in breakdown characteristics were observed in both 1J and 3J cells.

but a loss of current around 0.9 V in the SiGeSn-based devices serves to lower the fill factor to 73.7%. To help estimate the relative contributions of the subcells to the overall light I - V profile, the light I - V curves for the InGaP/GaAs/Ge control and InGaP/GaAs/SiGeSn 3J cell as well as the 1J forward bias dark I - V were fitted using a phenomenological single-diode model and the results shown by the solid lines in Figs. 7 and 8.

In the 3J cell configuration, it was assumed that the 1J Ge and SiGeSn diode profiles are representative of the internal junctions, resulting in relative contributions of 0.21 V for SiGeSn and 0.23 V for Ge. This left the remaining difference in voltage to be accounted for by the InGaP and InGaAs junction as 2.25 V for the 3J-SiGeSn cell and 2.13 V for the 3J-Ge control cell. However, the most notable feature in the 3J-SiGeSn light I - V curve is the inflection around 0.9 V that arises from reverse bias breakdown of the SiGeSn cell.

This can be understood by considering the different internal biases that exist across the subcells. At short circuit, only the cell terminals are at equal potential, but internally the sub cells will be biased according to their relative levels of photogeneration. The SiGeSn junction being the low voltage, current-limiting junction will be pushed into reverse bias and passes sufficient reverse current to allow the full photocurrent from the top two

cells to pass. At higher cell biases, the SiGeSn junction moves toward forward bias, becomes rectifying again, and restricts the current flow to the internal photogeneration, bringing about the kink in the I - V curve around 0.9 V in Fig. 7. To illustrate this point, the reverse bias SiGeSn subcell current required to fit the inflection in Fig. 7 was estimated and shown as a solid line on the current voltage graph. In Fig. 8, the estimated SiGeSn subcell dark I - V from the 3J device is plotted together with a representative dark I - V curve measured from a 1J SiGeSn cell. A range of subcell reverse bias breakdown profiles were measured from the 1J devices, so the difference observed is not surprising. Increasing photogenerated current in the SiGeSn subcell through greater SiGeSn layer thickness would mitigate the effect of this behavior on overall cell performance, although increasing the reverse bias breakdown voltage would also be desirable. Both devices show comparable series resistance response suggesting that the SiGeSn exhibits favorable carrier transport properties through the device.

V. SUMMARY

A SiGeSn subcell was integrated into a multijunction architecture, although significant further optimization is required, and some reverse bias leakage through the SiGeSn is evident from the light I - V results from the 3J device. EQE and light I - V device results for both 1J and 3J devices based on SiGeSn/Ge wafers are presented and modeled. The devices show strong EQE performance with the 1J and 3J devices exhibiting peak quantum efficiencies in excess of 80% and 70%, respectively, which were successfully modeled to establish a lower bound to the minority carrier diffusion length of 5 μm . Modeling indicates that the subcell photocurrent is presently limited by the subcell thickness. The open-circuit voltage of the SiGeSn subcell presently falls short of that of Ge, with the 1J Ge cell producing 0.261 V and SiGeSn producing 0.225 V. This is attributed to the presence of significant subbandgap tail states and excessive bulk recombination, which can be addressed through refined device design and epitaxial growth. Nevertheless, the results confirm that the SiGeSn ternary compounds are viable semiconductor alloys, which allow growth and fabrication of lattice-matched subcells with 1.0-eV bandgaps. These subcells can be either inserted or substituted into currently used multijunction cell structures without any significant changes.

ACKNOWLEDGMENT

T. Thomas would like to acknowledge EPSRC CASE sponsorship from IQE plc.

REFERENCES

- [1] P. Patel *et al.*, "Initial results of the monolithically grown six-junction inverted metamorphic multi-junction solar cell," in *Proc. IEEE 38th Photovoltaic Spec. Conf.*, Jun. 2012, pp. 1–4. [Online]. Available: <http://ieeexplore.ieee.org/lpdocs/epic03/wrapper.htm?arnumber=6656717>

- [2] AzurSpace Solar Power (GMBH), "Concentrator Triple Junction Solar Cell," 2015. [Online]. Available: http://www.azurspace.com/images/products/DB_4356-00-00_3C44_AzurDesign_5.5x5.5_2015-04-02.pdf
- [3] F. Dimroth *et al.*, "Four-junction wafer-bonded concentrator solar cells," *IEEE J. Photovoltaics*, vol. 6, no. 1, pp. 343–348, Jan. 2016.
- [4] A. Aho, A. Tukiainen, V. Polojärvi, and M. Guina, "Performance assessment of multijunction solar cells incorporating GaInNAsSb," *Nanoscale Res. Lett.*, vol. 9, no. 61, pp. 1–7, 2014.
- [5] K. Uesugi, S. Kuboya, S. Sanorpm, and K. Onabe, "Characterization of InGaAsN solar-cell structures on Ge substrates," *Phys. Status Solidi (C)*, vol. 11, nos. 3/4, pp. 561–564, 2014. [Online]. Available: <http://doi.wiley.com/10.1002/pssc.201300488>.
- [6] V. Sabnis, H. Yuen, and M. Wiemer, "High-efficiency multijunction solar cells employing dilute nitrides," in *Proc. AIP Conf.*, 2012, vol. 1477, pp. 14–19. [Online]. Available: <http://scitation.aip.org/content/aip/proceeding/aipcp/10.1063/1.4753823>
- [7] S. Kurtz *et al.*, "InGaAsN solar cells with 1.0 eV band gap, lattice matched to GaAs," *Appl. Phys. Lett.*, vol. 74, no. 1999, pp. 729–731, 1999.
- [8] K. Volz *et al.*, "Material Development for Improved 1eV (GaIn)(NAs) Solar Cell Structures," *J. Sol. Energy Eng.*, vol. 129, p. 266, Aug. 2007.
- [9] J. F. Geisz *et al.*, "High-efficiency GaInPGeAsInGaAs triple-junction solar cells grown inverted with a metamorphic bottom junction," *Appl. Phys. Lett.*, vol. 91, no. 2, pp. 10–13, 2007.
- [10] R. A. Soref and C. H. Perry, "Predicted band gap of the new semiconductor SiGeSn," *J. Appl. Phys.*, vol. 69, no. 1, p. 539, 1991. [Online]. Available: <http://scitation.aip.org/content/aip/journal/jap/69/1/10.1063/1.347704>
- [11] G. Sun, R. A. Soref, and H. H. Cheng, "Design of an electrically pumped SiGeSn/GeSn/SiGeSn double-heterostructure midinfrared laser," *J. Appl. Phys.*, vol. 108, no. 3, 2010.
- [12] Y.-Y. Fang *et al.*, "Molecular-based synthetic approach to new group IV materials for high-efficiency, low-cost solar cells and Si-based optoelectronics," *J. Am. Chem. Soc.*, vol. 130, no. 47, pp. 16095–16102, 2008.
- [13] R. Roucka, A. Clark, and B. Landini, "Si-Ge-Sn alloys with 1.0 eV gap for CPV multijunction solar cells," in *Proc. 12th Int. Conf. Concentrator Photovoltaic Syst.*, 2015, p. 040008. [Online]. Available: <http://scitation.aip.org/content/aip/proceeding/aipcp/10.1063/1.4931519>
- [14] J. Nelson, *The Physics of Solar Cells*. London, U.K.: Imperial College Press, 2003.
- [15] V. R. D'Costa *et al.*, "Sn-alloying as a means of increasing the optical absorption of Ge at the C- and L-telecommunication bands," *Semiconductor Sci. Technol.*, vol. 24, no. 11, p. 115006, 2009. [Online]. Available: <http://stacks.iop.org/0268-1242/24/i=11/a=115006?key=crossref.686f03a0e c97df7d2058cfe00643e9c1>
- [16] M. Fuhrer, D. Farrell, and N. Ekins-Daukes, "CPV modelling with Solcore: An extensible modelling framework for the rapid computational simulation and evaluation of solar cell designs and concepts," in *Proc. AIP Conf.*, 2013, vol. 1556, no. 1, pp. 34–37. [Online]. Available: <http://scitation.aip.org/content/aip/proceeding/aipcp/10.1063/1.4822193>
- [17] TS-Space Systems Unisim Compact - User Manual, *TS-Space Systems Unisim Compact—User Manual*, TS-Space Sys., Marlow, U.K., 2016.
- [18] U. Rau, "Reciprocity relation between photovoltaic quantum efficiency and electroluminescent emission of solar cells," *Phys. Rev. B—Condensed Matter Mater. Phys.*, vol. 76, no. 8, pp. 1–8, 2007.
- [19] R. R. King *et al.*, "Bandgap-voltage offset and energy production in next-generation multijunction solar cells," in *Proc. 5th World Conf. Photovoltaic Energy Convers. 25th Eur. Photovoltaic Sol. Energy Conf.*, 2010, pp. 6–10.

Authors' photographs and biographies not available at the time of publication.